Front. Optoelectron. 2019, 12(3): 317–323
https://doi.org/10.1007/s12200-019-0861-1

RESEARCH ARTICLE

Edge detection on terahertz pulse imaging of dehydrated cutaneous malignant melanoma embedded in paraffin

Jiayu LI, Yijun XIE, Ping SUN (✉)

Beijing Key Laboratory of Applied Optics, Department of Physics, Beijing Normal University, Beijing 100875, China

Abstract Terahertz pulse imaging of cutaneous malignant melanoma dehydrated by ethanol and embedded in paraffin was carried out across a frequency range of 0.2–1.4 THz. First, the tissue images based on the time-domain electric-field amplitude information were acquired. Then the areas of normal and cancerous tissues were determined using multi-scale, multi-azimuth and multi-structural element mathematical morphology. The physical meaning of the image was analyzed by calculation of the refractive index and absorption coefficient of cutaneous malignant melanoma in different areas. The refractive index of both normal and cancerous tissues showed anomalous dispersion. The refractive index of cancerous tissues tended to vary between 0.2 and 0.7 THz, while that of normal and fat tissues remain almost unchanged. The absorption of cancerous tissues was higher, with a maximum at 0.37 THz. We concluded that both the refractive index and absorption coefficient differ considerably between normal and cancerous tissues, and the areas of normal and abnormal tissues can be identified using THz pulse imaging combined with mathematical morphology. The method for edge detection of terahertz pulse imaging of cutaneous malignant melanoma provides a reference for the safe surgical removal of malignant tumors.

Keywords terahertz pulse imaging, edge detection, mathematical morphology, cutaneous malignant melanoma, refractive index, absorption coefficient

1 Introduction

Terahertz time-domain pulse imaging (THz-TPI) is an emerging imaging technology with high signal-to-noise ratio and high sensitivity. It has been used in the medical and biological imaging fields in recent years [1–6]. It offers the following advantages [7]: The frequency of this THz radiation is 10^{12} Hz and the power order of magnitude is meV, so it causes almost no ionization damage to human tissue. For contrast, X-ray radiation has a frequency of 10^{20} Hz and the power order of magnitude is MeV. The wavelength of THz is 0.03–3 mm, which is larger than the size of scattered particles in the tissue. When THz waves interact with tissues, there is only a weak scattering effect. In this way, it outperforms near-infrared optical imaging, which has a wavelength of 10^2–10^3 nm. Because TPI uses the coherence technique to record the electrical fields associated with the THz waves, the amplitude and phase of tissues can be detected simultaneously. With the amplitude and phase, the refractive index and absorption coefficient of the detected tissue can be acquired. This enables TPI to provide both structural and functional information, due to chemical specificity, enabling the investigation of both morphological and chemical changes. However, one should note that the structural and the chemical information are convolved in a single reflected pulse and can only be separated if one is known a priori [8]. For these reasons, TPI can indicate changes in tissue morphology and chemical composition to detect and differentiate different biological tissues.

In recent years, the number of cases of cutaneous cancer has continued to grow. Annually, there are 2–3 million diagnoses of nonmelanoma cutaneous cancer and more than 130 thousand diagnosis of cutaneous malignant melanoma (CMM) globally [9]. CMM is a cutaneous tumor caused by abnormal hyperplasia of melanoma. It features a high degree of malignancy, high rates of metastasis and recurrence, poor prognosis, and high mortality. Currently, typical CMM is diagnosed using the ABCDE standard [10] and abnormality is classified according to the latest TNM staging standard [11] issued by the American Joint Committee on Cancer (AJCC). Through diagnosis and staging, doctors can identify the extent of the surgery needed to remove the primary CMM lesion. However, due to the cytological morphology of

Received July 31, 2018; accepted October 24, 2018

E-mail: pingsun@bnu.edu.cn

CMM, the diversity of its histopathology, atypical tumors, and tumors without melanin, missed diagnosis and misdiagnoses are likely [12]. Some research suggests that TPI can be used to distinguish abnormal from normal tissues, for example, Woodward et al. [13] differentiated basal cell carcinoma (BCC), inflammatory tissues from normal tissues by analyzing the contrast in the image. Wallace et al. [14] interpreted the difference in contrast as the difference in water content in specific tissues, which causes differences in their refractive index and absorption coefficients. Arbab et al. [6] performed a TPI experiment on rat skin. The results showed that the reflection rate of burned tissue is higher than that of normal tissues between 0.5 and 0.7 THz. Sim et al. [15] imaged the oral melanoma using TPI within the temperature range of −20°C–20°C. They found melanoma could be identified clearly in the image and the contrast of the image increased as temperature decreased. Fan et al. [16] performed a TPI experiment on the trauma tissue of the human arm. The results showed that TPI can be used to distinguish scars from normal skin. So TPI has potential applications in the detection of CMM.

Surgical resection is currently the most effective treatment for malignant melanoma. Therefore, identifying the extent of the primary lesion and removing the nidus accurately can decrease the likelihood of tumor cells in the margins and tumor recurrence [17]. However, the identification of tumor area is still open problems. Mathematical morphology describes the essential shape morphological characteristics of the image through a series of operators (erosion, dilation, opening and closing) using a certain form structural elements [18]. At present, mathematical morphology has been a powerful nonlinear technique for image analysis [19–21].

In this study, we selected the dehydrated CMM tissue as sample in order to exclude changes in water content and investigate the structural changes [22]. Reflective TPI was performed on CMM tissues and the edges of the cancerous tissue were determined using multi-scale, multi-azimuth and multi-structural element mathematical morphology, which provides a reference for CMM surgery. This study shows the feasibility of using the mathematical morphology approach, a simple and rapid method, for extracting relevant edges in CMM images.

2 Sample preparation and THz pulse imaging

2.1 Sample preparation

Figure 1 shows the human bulk CMM tissue immersed in formalin. The bulk tissue had been infiltrated by subcutaneous tissue and a lot of stellate ganglions became visible. Based on the clinical and pathological results and AJCC staging standards, the CMM was classified as stage III and with regional metastasis. That is, the regional lymph node involvement and deep tissue infiltration. The samples were prepared as follows: 1) Sectioning: a 2.5 mm section was cut along cross-section of the tissue, which also included the epidermis, dermis, fat, and cancerous tissue; 2) Dehydration: sections were placed in a small, narrow-mouthed bottle. Serial concentrations of ethanol served as dehydrating reagents and there was an 8:1 ratio of ethanol to tissue with respect to volume. The dehydration was carried out in steps from a low concentration of ethanol to higher concentrations. Table 1 shows the different time when the samples were immersed in each concentration of ethanol. One dehydrated sample with a thickness of 1.5 mm is shown in Fig. 2(a); 3) Embedding: the dehydrated tissue sections were placed in melted paraffin and allowed to naturally cool down. Figure 2(b) shows the sample with a thickness of 1.5 mm embedded in paraffin. The other 4 samples were similar. The process of sample preparation was performed at 15°C.

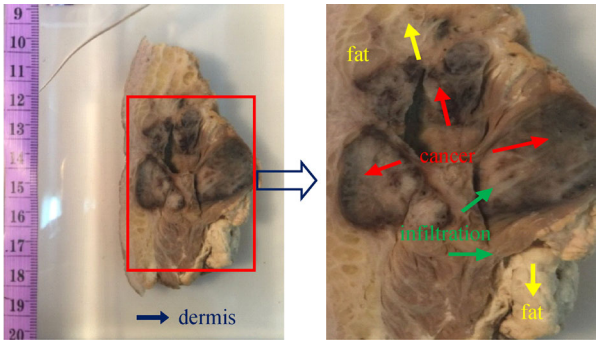

Fig. 1 Bulk tissue of human cutaneous malignant melanoma immersed in formalin

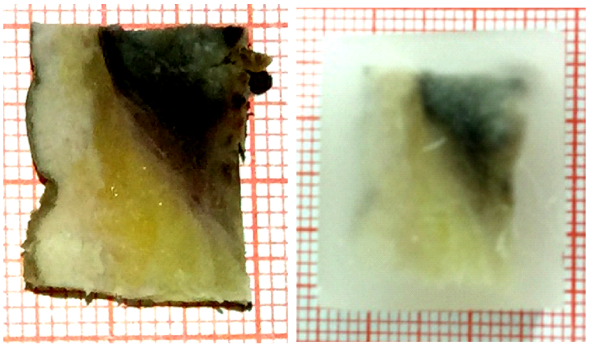

(a) (b)

Fig. 2 Tissue section of human cutaneous malignant melanoma. (a) After dehydration with a thickness of 1.5 mm; (b) embedded in paraffin with a depth of 0.84 mm

Table 1 Concentration and time for dehydration

dehydration level	1	2 (two times)	3 (two times)	4
ethanol concentration/%	80	95	98	98
time/min	110	100	50	40

2.2 THz pulse imaging

A reflective TPI system (TAS7500IM, Advantest (China) Management Limited Co.) was used in the imaging experiment ranged from 0.2–1.4 THz. The cutaneous tissue sample was shown in Fig. 2(b). Before imaging experiment, a reference pulse image of air was tested with a total reflective mirror. The pulse image of paraffin was also tested and the results show that THz waves can penetrate paraffin, and there was no characteristic absorption. The optical path of THz wave was purged by dry air in order to remove water vapor and keep the relative humidity 3.0% during the whole experiment. Simultaneously, the laboratory was at a constant temperature of 15°C.

Figure 3 shows the optical path. A beam of THz wave reached to the surface of sample and propagated through the paraffin with a thickness of 0.84 mm. Then the tissue reflected the THz wave. The first peak of THz wave is the reflective signal of paraffin on the surface of the sample, i.e., E_1 and the second peak is the reflective signal of tissue at the interface between the paraffin and the cutaneous tissue, i.e., E_2. We therefore selected the maximum electrical field of the second peak for imaging. A total of 877 points of the sample were tested and each point had a step of 0.3 mm. Figure 4(a) shows the sample scanning area and Fig. 4(b) shows the imaging result. The result was shown in pseudo color in order to remove observer bias in classifying information. As shown in Fig. 4, comparison of the pseudo color image and the dehydrated cutaneous tissue before embedding showed similar spatial distribution. The blue area corresponds to fatty tissue. The red and green areas roughly corresponded to the cutaneous tissue tumor and the infiltrated areas.

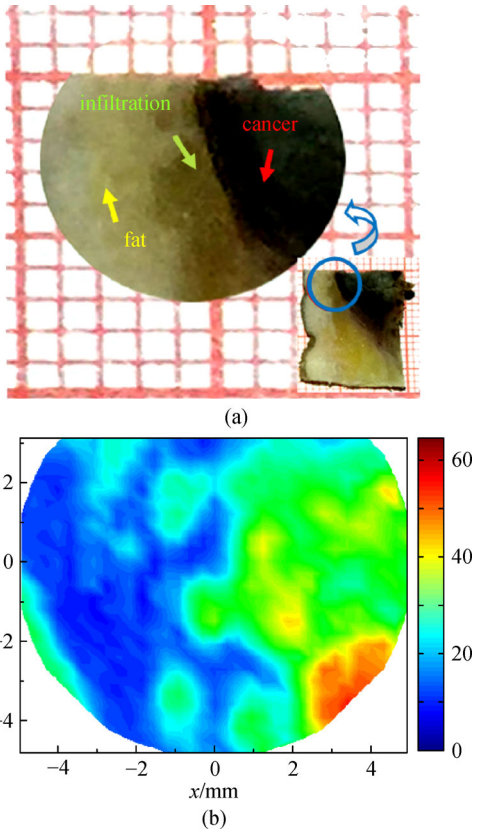

Fig. 4 Scanning aera and imaging result of tissue section of human cutaneous malignant melanoma. (a) Scanning aera of dehydrated tissue section before embedding; (b) pseudo-color image of the reflective time-domain signal of tissue at the interface between the paraffin and the cutaneous tissue

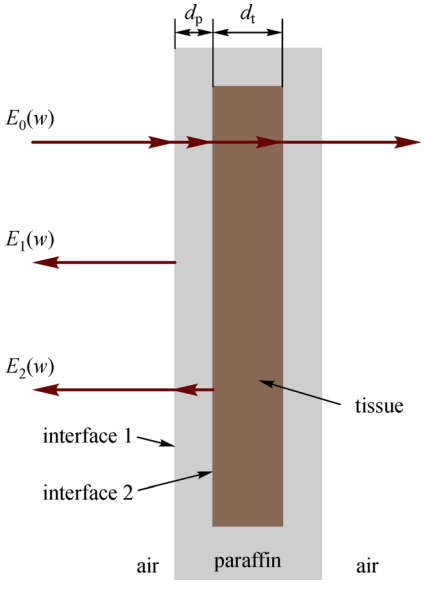

Fig. 3 Schematic diagram of light propagating. E_0 is the incident light; E_1 is the reflective signal of paraffin on the surface of the sample; E_2 is the reflective signal of tissue at the interface between the paraffin and the cutaneous tissue

3 Edge detection and analysis of results

3.1 Edge detection

Greyscale distribution in biomedical images is determined by the differences in the characteristic parameters of human tissues. Since the differences were so slight, the image contrast is low. In this study, multi-scale, multi-azimuth and multi-structural element mathematical morphology [18] was used to detect edge of image. The different structural elements have specific effects on the edge sensitivity and the structural elements with different scales and azimuths have inhibiting effects on noise. With large-scale structural elements, global information concerning edges can be obtained, while detailed information can be obtained using small-scale structural elements [18]. The final edge image can be obtained by weighting and integrating the edge information at different scales and

azimuths according to their adaptive weight. In this study, a 3 × 3 diamond structural element and 4 × 4 rectangular structural element were selected to extract the TPI of cutaneous tissues from 6 angles, i.e., 0°, 30°, 45°, 60°, 90°, and 135°. Figure 5 shows an extracted edge of the image from Fig. 4(b). It can be seen that the extracted edge can be used to distinguish the different regions with different colors.

3.2 Analysis of results

We analyzed the total of 877 points of the sample. Here we take only one example to present the results. A polyline was selected and are shown in Fig. 5, including seven specific points, 1(cancer), 2(cancer), 3(cancer), 4(cancer), 5(cancer), 6(infiltration), and 7(fat) including the different information of normal and abnormal parts of tissue. The time-domain signals of these points are Fourier-transformed to obtain the frequency spectrum of the corresponding points, as shown in Fig. 6. In Fig. 6, the black solid line is the spectrum of paraffin. The spectral curves of the cutaneous tissues and paraffin intersect at about 0.53 THz. The areas with high degree of cancerous malignant melanoma tissue showed higher frequency-domain amplitude than normal tissues such as fat. The closer to the cancerous tissue areas the point was, the higher the amplitude was at the low-frequency area. This conclusion is consistent with the result of the literature [6]. The refractive indices and the absorption coefficients of the tested samples can be extracted according to the frequency spectrum.

The method [23] to extract the complex refractive index of cutaneous tissue was used in this work. During the application of the method, silica glass was converted to paraffin and water was converted to cutaneous tissues. Figures 7(a) and 7(b) show the refractive index and the absorption coefficient of the 7 specific points on the polyline, respectively. The results show following characteristics: 1) Refractive index: the refractive index of normal and cancerous tissues decreases with increasing frequency and tends toward 1.2, showing anomalous dispersion. The refractive index of cancerous tissues (points 1–6) fluctuates greatly within the low frequency of 0.2–0.7 THz, but fatty tissues (point 7) remain near 1.2. 2) Absorption coefficient: the absorption of normal and fatty tissues is low but that of cancerous tissues is high, showing a maximum at 0.37 THz. The results of calculation indicate an obvious difference between the refractive index and absorption coefficient of normal and cancerous tissues at some specific frequencies.

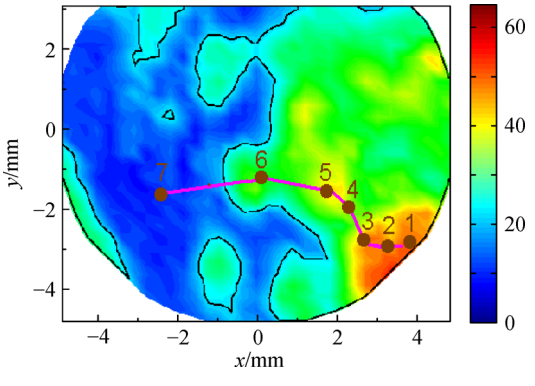

Fig. 5 Extracted edge of the image from Fig. 4(b) and specific points in different image regions including the different information of fat, infiltration and cancer

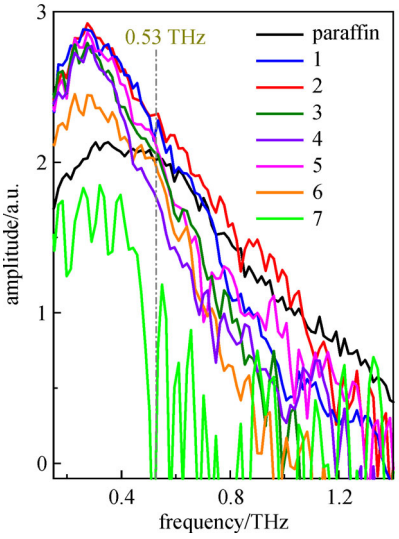

Fig. 6 Fourier-transformed spectrum of specific points on tissue section of human cutaneous malignant melanoma

From the perspective of histopathology: Typical CMM appears brown or gray-black, nodular or plaque, and the lesions appear coarse, taking on a fine granular shape or flake desquamation. Its edge is irregular and the diameter is greater than 6 mm. All these characteristics are consistent with ABCDE standards [10]. Therefore, the tissues conformed to ABCDE standard are regarded as highly suspected CMM. Figure 8(a) is a typically clinical CMM photo [24]. Under a microscope, a CMM pathological section shows abnormal hyperplasia of melanocytes. This leads to cell nests in the epidermis or the boundaries between epidermis and dermis. These cell nests differ in size and can mix together. There are several degrees of variation among the size and shapes of melanocytes in the nest and of its nucleus. Mitosis is very common and there are pigment granules in the cytoplasm of tumor cells. In invasive CMM, tumor cells invade the dermis and subcutaneous tissue [25,26]. Figure 8(b) is the case of propagation along the surface of melanoma pathological conditions [27]. As shown in Fig. 8(b), the pigment particles in the melanin cell cytoplasm disperse like dust. The cutaneous tissue samples in this study were invasive

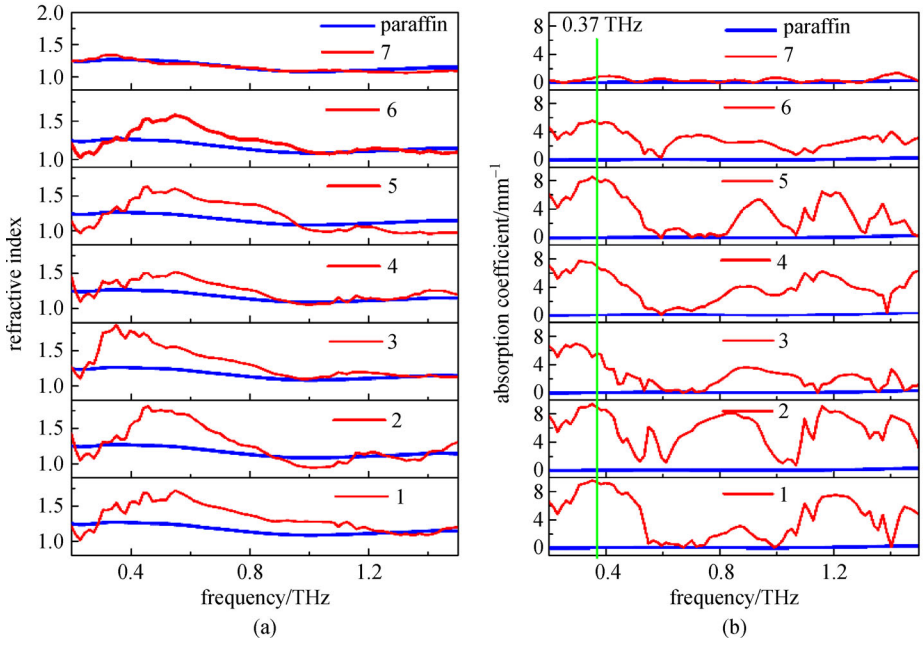

Fig. 7 Refractive index and absorption coefficient of different specific points on Polyline I. (a) Refractive index; (b) absorption coefficient

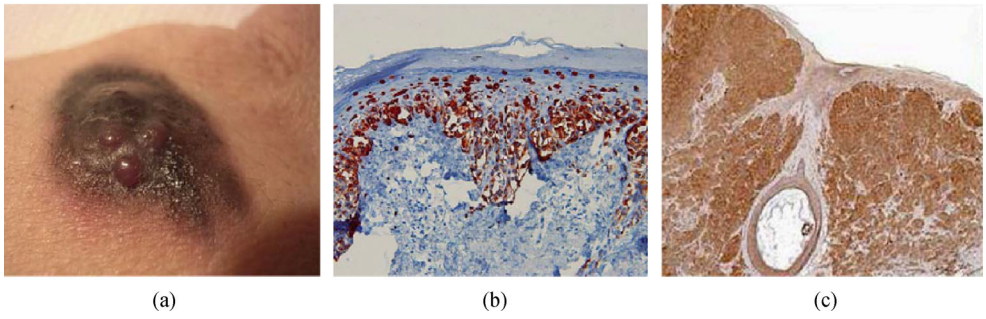

Fig. 8 Clinical manifestations of cutaneous malignant melanoma. (a) Cutaneous malignant melanoma with brown plaques [24]; (b) cell nests formation in the epidermis and dermis [27]; (c) immunohistochemical expression of NRP2 [31]

CMM; From the perspective of immunohistochemistry, proteins found in CMM cells, such as CD10 [28], P16 [29], Ki-67 [30], and NRP2 [31], showed some degree of positive expression. Figure 8(c) is the case of NRP2 melanoma positive expression [31]. These analyses indicates that when tissues get cancerous, the structure and composition of the tissues and the cells in the tissue changes. This changes the refractive index of representable structure and the absorption coefficient of representable composition. If changes in the refractive index and absorption coefficient are detected, the changes in the structure and composition of the tissues or the cells can be assessed to determine whether the tissue sample is cancerous or not.

4 Conclusions

Terahertz pulse imaging was performed on the dehydrated tissue section of cutaneous malignant melanoma based on multi-scale, multi-azimuth and multi-structural element mathematical morphology to reduce the interference of noise on the edge detection and to facilitate relatively accurate determination of the areas of normal and cancerous tissues. By calculating the refractive index and the absorption coefficient of cutaneous malignant melanoma at different locations, the following conclusions can be drawn: the refractive index of both normal and cancerous tissues have shown a law of anomalous dispersion. The refractive index of cancerous tissues

fluctuated considerably in low frequency while that of normal and fat tissues remained roughly the same. Normal and fatty tissues showed only slight absorption, but cancerous tissues showed much higher absorption than the normal one, with a maximum of about 0.37 THz. With THz band and the conclusion that there is an obvious difference between the refractive indexes and the absorption coefficients of normal and cancerous tissues, the areas of normal and abnormal tissues can be distinguished using THz pulse imaging combined with mathematical morphology. The method for extracting edge of CMM image of this study can provide a reference for surgical removal of malignant tumors.

Acknowledgements This work was supported by the National Natural Science Foundation of China (Grant No. 61371055).

References

1. Bajwa N, Au J, Jarrahy R, Sung S, Fishbein M C, Riopelle D, Ennis D B, Aghaloo T, St John M A, Grundfest W S, Taylor Z D. Non-invasive terahertz imaging of tissue water content for flap viability assessment. Biomedical Optics Express, 2017, 8(1): 460–474
2. Grootendorst M R, Fitzgerald A J, Brouwer de Koning S G, Santaolalla A, Portieri A, Van Hemelrijck M, Young M R, Owen J, Cariati M, Pepper M, Wallace V P, Pinder S E, Purushotham A. Use of a handheld terahertz pulsed imaging device to differentiate benign and malignant breast tissue. Biomedical Optics Express, 2017, 8(6): 2932–2945
3. Yamaguchi S, Fukushi Y, Kubota O, Itsuji T, Ouchi T, Yamamoto S. Brain tumor imaging of rat fresh tissue using terahertz spectroscopy. Scientific Reports 2016, 6: 30124
4. Oh S J, Kim S H, Ji Y B, Jeong K, Park Y, Yang J, Park D W, Noh S K, Kang S G, Huh Y M, Son J H, Suh J S. Study of freshly excised brain tissues using terahertz imaging. Biomedical Optics Express, 2014, 5(8): 2837–2842
5. Tewari P, Kealey C P, Bennett D B, Bajwa N, Barnett K S, Singh R S, Culjat M O, Stojadinovic A, Grundfest W S, Taylor Z D. *In vivo* terahertz imaging of rat skin burns. Journal of Biomedical Optics, 2012, 17(4): 040503
6. Arbab M H, Dickey T C, Winebrenner D P, Chen A, Klein M B, Mourad P D. Terahertz reflectometry of burn wounds in a rat model. Biomedical Optics Express, 2011, 2(8): 2339–2342
7. Park G S, Kim Y H, Han H, Han J K, Ahn J, Son J H, Park W Y, Jeong Y U. Convergence of terahertz sciences in biomedical systems. Berlin: Springer, 2012, 351
8. Wallace V P, Macpherson E, Zeitler J A, Reid C. Three-dimensional imaging of optically opaque materials using nonionizing terahertz radiation. Journal of the Optical Society of America A, Optics, Image Science, and Vision, 2008, 25(12): 3120–3133
9. World Health Organization. http://www.who.int/bulletin/volumes/87/8/09-030809/zh/
10. Dzwierzynski W W. Managing malignant melanoma. Plastic and Reconstructive Surgery, 2013, 132(3): 446e–460e
11. Perera E, Gnaneswaran N, Jennens R, Sinclair R. Malignant Melanoma. Healthcare (Basel, Switzerland), 2013, 2(1): 1–19
12. Grant-Kels J M, Bason E T, Grin C M. The misdiagnosis of malignant melanoma. Journal of the American Academy of Dermatology, 1999, 40(4): 539–548
13. Woodward R M, Cole B E, Wallace V P, Pye R J, Arnone D D, Linfield E H, Pepper M. Terahertz pulse imaging in reflection geometry of human skin cancer and skin tissue. Physics in Medicine and Biology, 2002, 47(21): 3853–3863
14. Wallace V P, Fitzgerald A J, Pickwell E, Pye R J, Taday P F, Flanagan N, Ha T. Terahertz pulsed spectroscopy of human Basal cell carcinoma. Applied Spectroscopy, 2006, 60(10): 1127–1133
15. Sim Y C, Ahn K M, Park J Y, Park C S, Son J H. Temperature-dependent terahertz imaging of excised oral malignant melanoma. IEEE Journal of Biomedical and Health Informatics, 2013, 17(4): 779–784
16. Fan S, Ung B S Y, Parrott E P J, Wallace V P, Pickwell-Macpherson E. *In vivo* terahertz reflection imaging of human scars during and after the healing process. Journal of Biophotonics, 2017, 10(9): 1143–1151
17. Rath T. Malignant melanoma. European Surgery, 2006, 38(2): 145–148
18. Shih F. Mathematical Morphology. London: Wiley-IEEE Press, 2010, 3: 63
19. Dufour A, Tankyevych O, Naegel B, Talbot H, Ronse C, Baruthio J, Dokládal P, Passat N. Filtering and segmentation of 3D angiographic data: advances based on mathematical morphology. Medical Image Analysis, 2013, 17(2): 147–164
20. Merazi-Meksen T, Boudraa M, Boudraa B. Mathematical morphology for TOFD image analysis and automatic crack detection. Ultrasonics, 2014, 54(6): 1642–1648
21. Li Y, Liang X, Zuo M J. A new strategy of using a time-varying structure element for mathematical morphological filtering. Measurement, 2017, 106: 53–65
22. Sy S, Huang S, Wang Y X, Yu J, Ahuja A T, Zhang Y T, Pickwell-MacPherson E. Terahertz spectroscopy of liver cirrhosis: investigating the origin of contrast. Physics in Medicine and Biology, 2010, 55(24): 7587–7596
23. Huang S Y, Wang Y X J, Yeung D K W, Ahuja A T, Zhang Y T, Pickwell-Macpherson E. Tissue characterization using terahertz pulsed imaging in reflection geometry. Physics in Medicine and Biology, 2009, 54(1): 149–160
24. Wortsman X, Wortsman J. Clinical usefulness of variable-frequency ultrasound in localized lesions of the skin. Journal of the American Academy of Dermatology, 2010, 62(2): 247–256
25. Higgins H W 2nd, Lee K C, Galan A, Leffell D J. Melanoma *in situ*: Part I. Epidemiology, screening, and clinical features. Journal of the American Academy of Dermatology, 2015, 73(2): 181–190, quiz 191–192
26. Kelleher F C, McArthur G A. Targeting NRAS in melanoma. Cancer Journal (Sudbury, Mass.), 2012, 18(2): 132–136
27. Forman S B, Ferringer T C, Peckham S J, Dalton S R, Sasaki G T, Libow L F, Elston D M. Is superficial spreading melanoma still the most common form of malignant melanoma? Journal of the American Academy of Dermatology, 2008, 58(6): 1013–1020
28. Oba J, Nakahara T, Hayashida S, Kido M, Xie L, Takahara M, Uchi H, Miyazaki S, Abe T, Hagihara A, Moroi Y, Furue M. Expression

of CD10 predicts tumor progression and unfavorable prognosis in malignant melanoma. Journal of the American Academy of Dermatology, 2011, 65(6): 1152–1160

29. Al Dhaybi R, Agoumi M, Gagné I, McCuaig C, Powell J, Kokta V. p16 expression: a marker of differentiation between childhood malignant melanomas and Spitz nevi. Journal of the American Academy of Dermatology, 2011, 65(2): 357–363
30. Quatresooz P, Piérard G E. Malignant melanoma: from cell kinetics to micrometastases. Journal of the American Academy of Dermatology, 2011, 12(2): 77–86
31. Wititsuwannakul J, Mason A R, Klump V R, Lazova R. Neuropilin-2 as a useful marker in the differentiation between Spitzoid malignant melanoma and Spitz nevus. Journal of the American Academy of Dermatology, 2013, 68(1): 129–137

Ping Sun got bachelor degree of physics at Jilin University. In 2000, he got master degree of optics engineering at Beijing Institute of Technology. In 2004, he got Ph.D. degree of optics engineering at Beijing Institute of Technology. His research area includes biological photonics, digital holography and spectroscopy. His present work focus on the terahertz spectroscopy and imaging.